

gy to the next. This is consistent with a direct-reaction model.

The agreement with the DWBA for a large number of observables is satisfactory, considering the simplicity of the model. The fact that a first-order calculation whose basic ingredient is a one-channel optical potential gives a good account of the excitation curves suggests that it is not necessary to introduce additional *ad hoc* resonant amplitudes in order to fit the data, at least as far as the gross structure is concerned. Rather, corrections to the direct-reaction picture such as explicitly including other strongly coupled channels (e.g., the mutual excitation of both 2^+ states) or the inclusion of L -dependent absorption will probably be required to account for the details of the alignment of the residual 2^+ state.

Summarizing, measurements dependent on the alignment of the final state following inelastic excitation of the first 2^+ state in ^{12}C are reasonably well described over a wide energy range by a simple DWBA calculation, which also reproduces most of the gross structure observed in the total cross section. The measurements clearly illustrate the value of magnetic-substate population measurements for investigating the detailed predictions of nuclear-reaction models. Additional experimental work is under way in our laboratory to apply these techniques to other systems; in addition, we are presently investigating the refinements to the DWBA referred to above in order to

improve the correspondence between theory and experiment for the $^{12}\text{C} + ^{12}\text{C}$ system.

¹H. Emling, R. Nowotny, D. Pelte, and G. Schreider, Nucl. Phys. A211, 600 (1973).

²T. M. Cormier, J. Applegate, G. M. Berkowitz, P. Braun-Munzinger, P. M. Cormier, J. W. Harris, C. M. Jachcinski, L. L. Lee, Jr., J. Barrette, and H. E. Wegner, Phys. Rev. Lett. 38, 940 (1977); T. M. Cormier, C. M. Jachcinski, G. M. Berkowitz, P. Braun-Munzinger, P. M. Cormier, M. Gai, J. W. Harris, J. Barrette, and H. E. Wegner, Phys. Rev. Lett. 40, 924 (1978).

³R. L. Phillips, K. A. Erb, D. A. Bromley, and J. Weneser, Phys. Rev. Lett. 42, 566 (1979).

⁴Jae Y. Park, Walter Greiner, and Werner Scheid, Phys. Rev. C 16, 2276 (1977).

⁵Takehiro Matsuse, Yasuhisa Abe, and Yosio Kondō, Prog. Theor. Phys. 59, 1904 (1978); Yosio Kondō, Yasuhisa Abe, and Takehiro Matsuse, to be published.

⁶Osamu Tanimura, Institute for Nuclear Study, University of Tokyo, Report No. INS-313, 1978 (to be published).

⁷H. T. Fortune, S. C. Headley, L. R. Medsker, T. H. Braid, R. E. Segel, and K. Raghunathan, Phys. Rev. C 14, 1271 (1976).

⁸N. R. Fletcher, J. D. Fox, G. J. Kekelis, G. R. Morgan, and G. A. Norton, Phys. Rev. C 13, 1173 (1976).

⁹L. K. Fifield, R. W. Zurmühle, D. P. Balamuth, and J. W. Noé, Phys. Rev. C 8, 2203 (1973).

¹⁰P. D. Kunz, unpublished computer code.

¹¹W. Reilly, R. Wieland, A. Gobbi, M. W. Sachs, J. Hamer, R. H. Siemssen, D. Mingay, and D. A. Bromley, Nuovo Cimento A13, 897 (1973).

Evidence for Orbital Dispersion in the Fragmentation of ^{16}O at 90 and 120 MeV/Nucleon

K. Van Bibber, D. L. Hendrie, D. K. Scott, H. H. Weiman,
L. S. Schroeder, J. V. Geaga, S. A. Cessin, R. Treuhaft,
Y. J. Grossiord,^(a) and J. O. Rasmussen

Lawrence Berkeley Laboratory, University of California, Berkeley, California 94720

and

C. Y. Wong

Oak Ridge National Laboratory, Oak Ridge, Tennessee 37830

(Received 10 April 1979)

The parallel- and transverse-momentum distributions have been measured for fragments of $Z \geq 3$ produced by the fragmentation of ^{16}O at 90 and 120 MeV/nucleon. A strong anisotropy is observed with $\sigma_{p,1} \approx 200$ MeV/c for all fragments, which can be explained by considering the dispersion due to orbital deflection of the projectile prior to breakup.

The understanding of the reaction mechanism in projectile fragmentation has been long sought for. At relativistic energies with ^{12}C and ^{16}O projectiles, both the abrasion-ablation calculations and models of projectile excitation followed

by statistical decay adequately describe the isotope distributions.^{1,2} Further, it has been pointed out that there is an exact formal degeneracy between such models with regard to the fragment momentum distributions.³ Recent data for a

heavier projectile and lower energy (^{40}Ar , 213 MeV/nucleon) however, seem to favor a fast abrasion stage from relative isotopic and elemental yields.⁴ We report here, in the first heavy-fragment studies in the 100-MeV/nucleon region, an apparent anisotropy between p_{\perp} and p_{\parallel} . Incorporating the dispersion due to orbital deflection of the ^{16}O projectile by the combined Coulomb-nuclear field of the target with the usual dispersion due to the Fermi motion, we find good agreement with the p_{\perp} distributions. Although the present data also support either the abrasion-ablation model or the assumption of projectile excitation followed by statistical decay far from the target nucleus, better measurements at smaller p_{\perp} could discriminate between them and potentially prove to be a new tool for probing the interaction potential in the nuclear interior.

The average intensities and mid-target energies of the Bevalac ^{16}O beams were $\approx 5 \times 10^7$ /pulse at 92.5 ± 2 MeV/A and $\approx 10^8$ /pulse at 117.5 ± 2 MeV/A. Beam focusing and phase space were determined prior to each run by wire chambers at the target position and 2.5 m downstream, and during the run the beam profile was monitored and recorded pulse by pulse with the downstream wire chamber. Targets of thicknesses up to 235 mg/cm² Al and 500 mg/cm² Au were bombarded, and fragments of $Z=3-9$, $A=6-17$ were detected in a multielement silicon-germanium telescope. Double-differential cross sections $d^2\sigma/d\Omega dE$ were measured for each isotope at each angle. The energy spectra were narrow, essentially Gaussian, with a mean energy downshifted by ≈ 10 MeV/A from the beam velocity. The data have been corrected for multiple scattering, beam phase space, and longitudinal downshift in velocity due to the projectile-target interaction; the total contribution of these corrections was 7-10%. We fit the energy spectra and angular distributions assuming a Gaussian distribution in both p_{\parallel} and p_{\perp} in the projectile frame of reference:

$$P(\vec{p}) \propto \exp(-p_{\parallel}^2/2\sigma_{p_{\parallel}}^2 - p_{\perp}^2/2\sigma_{p_{\perp}}^2). \quad (1)$$

The distributions of $\sigma_{p_{\parallel}}$ as a function of fragment mass F are in good agreement with the parabolic form $\sigma_{p_{\parallel}}^2 = \sigma_0^2 F(A-F)/(A-1)$ expected from momentum conservation, and experimentally observed at higher energies.^{3,5} A and F are the projectile and fragment atomic numbers, respectively. At 92.5 MeV/A we find $\sigma_0 = 80$ MeV/c for the Au target, and 86 MeV/c for the Al, in good agreement with the value of 86 MeV/c found at 2.1 GeV/A, averaged over many targets.⁵

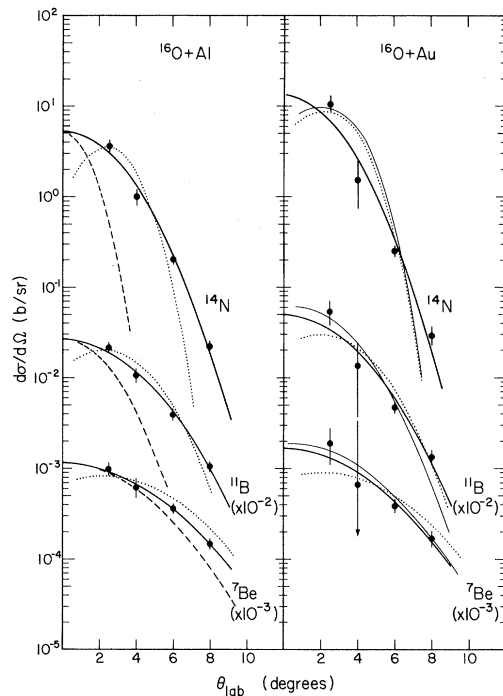


FIG. 1. Typical angular distributions for $^{16}\text{O}+\text{Al}$, $^{16}\text{O}+\text{Au}$ at 92.5 MeV/A. The solid curves are the best fit from Eq. (1); the dashed curves for $\sigma_{p_{\perp}}=86$ MeV/c. The dotted curves result from folding the deflection function with the momentum distribution due to the intrinsic nucleon motion; similarly for the fine lines, but under the abrasion-ablation assumption.

The situation with the distributions of $\sigma_{p_{\perp}}$ is rather different. An inspection of the angular distributions (see Fig. 1) reveals that they are significantly broader than expected from the Fermi motion alone. The solid curves are the best fits in $\sigma_{p_{\perp}}$ from Eq. (1); the dashed curves pertain to $\sigma_0 = 86$ MeV/c. Figure 2 shows the ensemble of all transverse-momentum widths, which are nearly all in excess of 200 MeV/c with an overall systematic increase with fragment mass. This behavior is in sharp contrast with that at 1.05 and 2.1 GeV/A where $\sigma_{p_{\parallel}} = \sigma_{p_{\perp}}$ to within 10%.

The origin of these surprisingly large widths may be understood if one notes that the projectile is subject to an orbital deflection due to its interaction with the target nucleus before fragmentation takes place. The large fragmentation cross section implies that a wide range of impact parameters contributes to this process, and as different impact parameters lead to different deflection angles, the orbital deflection gives an additional dispersion of the transverse momentum. Clearly the additional contribution to the

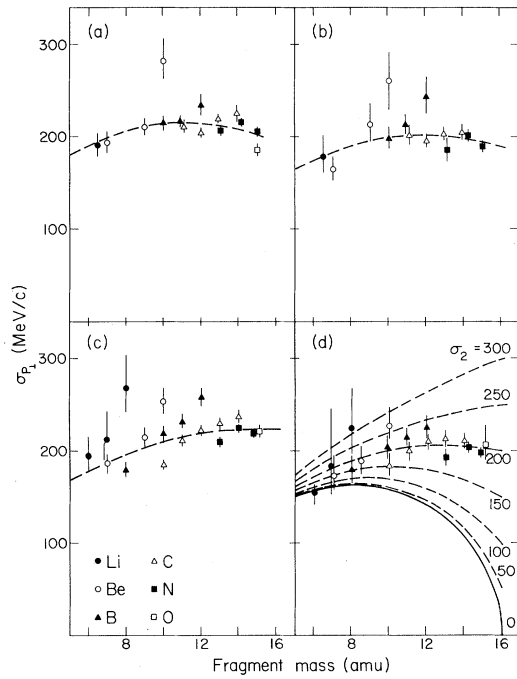


FIG. 2. Observed $\sigma_{p_{\perp}}$ for each isotope for (a) $^{16}\text{O} + \text{Al}$, 117.5 MeV/A; (b) $^{16}\text{O} + \text{Au}$, 117.5 MeV/A; (c) $^{16}\text{O} + \text{Al}$, 92.5 MeV/A; (d) $^{16}\text{O} + \text{Au}$, 92.5 MeV/A. For (a)–(c), the fitted curves are the best two-parameter fit (σ_1 and σ_2 both unconstrained; values found in Table I); curves in (d) are for $\sigma_1 = 78.9$ MeV/c; values of σ_2 from 0 to 300 MeV/c to show the presumed evolution of $\sigma_{p_{\perp}}$ as one goes from the extreme relativistic case to lower energies where the orbital dispersion of the projectile becomes significant.

width of $\sigma_{p_{\perp}}$ becomes more important the lower the energy of the projectile. Upon extending the derivations of Ref. 3 to include orbital deflection, we find

$$\sigma_{p_{\perp}}^2(F) = \frac{F(A-F)}{A-1} \sigma_1^2 + \frac{F(F-1)}{A(A-1)} \sigma_2^2, \quad (2)$$

where $\sigma_1^2 = \frac{1}{2} \langle \vec{p}_{I\perp}^2 \rangle = \sigma_0^2$ is the usual term due to the intrinsic nucleon motion, and $\sigma_2^2 = \frac{1}{2} \langle \vec{p}_{A\perp}^2 \rangle$ is the variance of transverse momentum of the projectile at the time of fragmentation.

The quality of the two-parameter fits according to Eq. (2) is evidently good. Table I contains the summary of the fitted and calculated values of σ_2 . Fitting the experimental $\sigma_{p_{\perp}}(F)$ according to Eq. (2), we fix $\sigma_1 = 80, 86$ MeV/c. However, when σ_1 is also allowed to be a free parameter, its value is equal within errors to $\sigma_{p_{\parallel}}$, convincing evidence that the functional form of Eq. (2) contains the essential physics. In Fig. 2, (a)–(c) show the best two-parameter fit (σ_1 not constrained; values in Table I); (d) shows the family of curves corresponding to one value of σ_1 , and values of σ_2 ranging from 0 to 300 MeV/c.

Having thus understood the average behavior of the widths, we seek a more detailed description of the angular distributions. We consider a simple model in which the projectile is first deflected through the Coulomb-nuclear potential and subsequently fragments. The angular distribution of any fragment is obtained by folding the

TABLE I. Summary of the fitted parameters σ_1 and σ_2 of Eq. (2) to the experimental $\sigma_{p_{\perp}}$. These are compared with our calculated values of σ_2 for $f=0.6$ and $R = r_0(A_1^{1/3} + A_2^{1/3})$, $r_0 = 1.2$ fm; $a = 0.6$ fm and V tabulated.

Target	$E_{1ab}(^{16}\text{O})$ (MeV/A)	σ_1 (MeV/c)	σ_2^{expt} (MeV/c)	σ_2^{theor} (MeV/c)	V (MeV)
Al	92.5	80	223.0 ± 2.3		
		86	215.2 ± 2.4		
Au	92.5	79.6 ± 2.1 ^a	223.5 ± 3.5	197.2	60 ^b
		80	198.1 ± 3.9		
Al	117.5	86	189.8 ± 4.0		
		78.9 ± 3.3 ^a	199.5 ± 5.8	193.6	85 ^b
Al	117.5	80	198.1 ± 2.6		
		86	192.5 ± 2.7		
Au	117.5	88.1 ± 2.2 ^a	192.5 ± 4.4	174.9	60
		80	188.2 ± 4.2		
		86	179.4 ± 4.3		
		80.3 ± 3.7 ^a	187.8 ± 6.7	169.6	85

^aTwo-parameter fit; σ_1 unconstrained.

^b v determined to reproduce the angular distributions at 92.5 MeV/A.

projectile angular distribution from the classical deflection function, $\theta(b)$, with the fragment momentum distribution due to the Fermi motion. The nuclear potential is taken to be of the Woods-Saxon form with radius parameter $r_0 = 1.2$ fm, diffusivity $a = 0.6$ fm, and a well depth to be determined. Both point charge and parabolic Coulomb potentials were used in the nuclear interior and the main difference appears to be at small angles for which no experimental data points are available. The only other input to the calculation is the fraction of the total cross section which appears as fragmentation, $f = \sigma_{\text{frag}}/\sigma_{\text{tot}}$. This value, 0.6 ± 0.1 for both targets,⁶ defines the range in impact parameter (b_1, R) over which the deflection function operates in a sharp-cutoff representation. Here R is the sum of target and projectile radii, $R = r_0(A_1^{1/3} + A_2^{1/3})$. In terms of the deflection function the variance σ_2^2 is given by $\sigma_2^2 = \frac{1}{2} b_A^2 \int_{b_1}^R N(b) \sin^2 \theta(b) db$, and $N(b) = 2b/(R^2 - b_1^2)$ is the weighting factor for the impact parameter. Implicit in the calculation is the assumption that the dispersion is principally refractive, or dynamic, rather than quantal; in the 100-MeV/A region, this can be shown to be reasonably satisfied.

The comparison of the experimental angular distributions with those resulting from the folding procedure (dotted line, Fig. 1) indicate that the shape of the angular distribution can be well reproduced by choosing a potential well depth of 65 MeV for the Al target and 85 MeV for Au, which are within the range of depths determined from optical-model analyses. Two aspects of these calculations deserve comment. The first is that for the larger fragment masses, the angular distributions are predicted to peak at a nonzero angle. Second, we observe that, while our choice of potentials reproduces the average falloff of the data with angle, the calculated angular distributions are slightly wider for the lighter fragments and narrower for the heavier fragments.

To examine to what degree this behavior may be due to an impact-parameter dependence of the final fragment mass, we have alternatively performed these calculations assuming an abrasion-ablation mechanism. Thus instead of the entire range of impact parameters (b_1, R) contributing equally to the calculated dispersion for all F , weighted only by $N(b)$, we now posit that the production of a fragment of mass F is associated with a mean impact parameter b_F . The b_F 's are calculated in the "clean-cut" geometry, and for each F the integration over impact parameters is

weighted further by a realistic smearing function,¹ of Gaussian form with full width 2 fm and mean b_F . These calculations for the Au target are depicted by the fine line in Fig. 1. Although several difficult questions are left unaddressed in this simple approach, it is clear that such an impact-parameter dependence would manifest itself most strikingly near 0° . On the other hand both the abrasion-ablation model and that of projectile excitation followed by decay far from the nuclear field of the target seem not to differ substantially in the tails of the angular distribution.

In summary, the large $\sigma_{p,1}$ observed in the fragmentation of ^{16}O in the vicinity of 100 MeV/A are well described by incorporating the dispersion due to orbital deflection of the projectile prior to fragmentation along with Fermi motion. The orbital dispersion is larger at 92.5 MeV/A than at 117.5 MeV/A as expected, and both experiment and theory diminish by the same ratio. The calculations (nonrelativistic) for the case of $^{16}\text{O} + \text{Au}$ at 400 MeV/A predict $\sigma_2 = 89$ MeV/c, suggesting that by 1.05 GeV/A the orbital dispersion term will have vanished entirely, and isotropy recovered. While present data cannot distinguish between excitation followed by decay far from the target, and abrasion-ablation mechanisms, measurements into 0° will be of greatest utility for reaction dynamics, and such measurements may prove to be a useful tool in probing the nucleus-nucleus potential for deep incursions of the target and projectile.

We thank the Bevatron operating crew for providing the low-energy beams, and acknowledge useful discussions with Peter Lindstrom, Douglas Greiner, Lance Wilson, Hank Crawford, Erwin Friedlander, and G. R. Satchler. The work was supported by the Nuclear Physics Division of the U. S. Department of Energy under Contract No. W-7405-ENG-48 and the Union Carbide Corporation.

^(a)Present address: Institut de Physique Nucleaire de Lyon, 43 Boulevard du 11 Novembre 1918, 69621 Villeurbanne, France.

¹J. Hüfner, K. Schäfer, and B. Schürmann, Phys. Rev. C **12**, 1888 (1975).

²V. K. Lukyanov and A. I. Titov, Phys. Lett. **57B**, 10 (1975); J. Hüfner, C. Sander, and G. Wolschin, Phys. Lett. **73B**, 289 (1978).

³A. S. Goldhaber, Phys. Lett. **53B**, 306 (1974).

⁴Y. P. Viyogi, T. J. M. Symons, P. Doll, D. E. Greiner, H. H. Heckman, D. L. Hendrie, P. J. Linstrom,

J. Mahoney, D. K. Scott, K. Van Bibber, G. D. Westfall, H. Wieman, H. J. Crawford, C. McParland, and C. K. Gelbke, *Phys. Rev. Lett.* **42**, 33 (1979).

⁵D. E. Greiner, P. J. Lindstrom, H. H. Heckman, Bruce Cork, and F. S. Bieser, *Phys. Rev. Lett.* **35**, 152 (1975).

⁶Isotope production cross sections as well as total fragmentation cross sections will be published at a

later time. While no total-reaction-cross-section data exist at this time in the 100-MeV/A range, accurate measurements exist at 2.1 GeV/A and a continuation formula is used to estimate the total reaction cross sections at 100 MeV/A [Paul J. Karol, *Phys. Rev. C* **11**, 1203 (1975)]. The variation with energy is expected to be small, the cross sections being essentially geometric at both energies.

Neutron Radii Determinations from the Ratio of π^- Elastic Scattering from $^{12,13}\text{C}$ and $^{16,18}\text{O}$

R. R. Johnson, T. Masterson, B. Bassalleck, W. Gyles, T. Marks, and K. L. Erdman
Physics Department, University of British Columbia, Vancouver, British Columbia V6T 1W5, Canada

and

A. W. Thomas and D. R. Gill
TRIUMF, Vancouver, British Columbia V6T 1W5, Canada

and

E. Rost and J. J. Kraushaar^(a)
University of Colorado, Boulder, Colorado 80309

and

J. Alster^(a)
Physics Department, Tel-Aviv University, Ramat Aviv, Israel

and

C. Sabev^(a)
CERN, 1211 Geneva, Switzerland

and

J. Arvieux^(a)
Institut des Sciences Nucléaires, Institut National de Physique Nucléaire et de Physique des Particules, F38044 Grenoble, France

and

M. Krell^(a)
Université de Sherbrooke, Sherbrooke, Québec J1K 2R1, Canada

(Received 7 May 1979)

Differential elastic cross-section ratios and absolute cross sections have been measured for $^{12,13}\text{C}$ at 29.2- and 49.5-MeV average π^- energy and for $^{16,18}\text{O}$ at 29.2 MeV. Range telescopes detected the scattered pions. The ratio data were compared with different optical-potential calculations to extract neutron radii of 2.35 ± 0.03 fm for ^{13}C and 2.81 ± 0.03 fm for ^{18}O , relative to the neutron radii of ^{12}C (2.31) and ^{16}O (2.60), respectively. Our studies indicate little sensitivity to the optical model used.

A long-standing question of nuclear structure concerns the neutron density distribution which is not nearly as well known as the proton distribution. Various methods have been applied but there are still major discrepancies between the results obtained by different techniques.¹ Here we consider a new method that involves the measurement of the angular distributions of elastically

scattered π^- at low energy from a pair of isotopes, one of which has reasonably well-established neutron and proton density distributions. We measured the ratio of the differential cross sections for the pair since both systematic errors in the data and uncertainties in the theory cancel to a large extent. In the low-energy region the π^-n elastic-scattering amplitude is much